Effect of lattice defects and temperature transition rates on the deuteride (hydride) particle morphology and phase transformation thermal hysteresis in niobium

1999 J. Phys.: Condens. Matter 11 7195

(http://iopscience.iop.org/0953-8984/11/38/301)

J. Phys.: Condens. Matter **11** (1999) 7195–7210. Printed in the UK PII: S0953-8984(99)02289-4

Effect of lattice defects and temperature transition rates on the deuteride (hydride) particle morphology and phase transformation thermal hysteresis in niobium

Brent J Heuser and W C Chen

University of Illinois, Department of Nuclear Engineering, Urbana, IL 61801, USA

Received 4 March 1999, in final form 22 June 1999

Abstract. Small-angle neutron scattering (SANS) measurements have been performed to investigate deuteride particle morphology and the phase transformation temperature hysteresis in low-concentration Nb–D alloys. Deformation either by cold rolling and or by previous deuteride cycling induced a coarse deuteride particle distribution. This observation is attributed to a more heterogeneous precipitation process facilitated by the dislocation defects and/or dislocation substructure. Deuteride precipitation in the deformed samples was observed immediately upon crossing the incoherent solvus during temperature reduction, again consistent with dislocation-aided nucleation. Deuteride dissolution was observed at the very onset of heating for the cold-rolled material, an observation unique among the samples characterized here. This is attributed to the availability of elastic accommodation energy for deuteride particles embedded in the severely work-hardened host matrix. In other words, the elastic energy assists dissolution, consistent with a theoretical model developed by Puls (1984 *Acta Metall.* **32** 1259–69). The effect of temperature reduction transition rates was also investigated. Rapid, direct cooling (at 2–3 K min^{-1}) resulted in a much finer deuteride particle distribution—a factor of 200 increase in the particle number density and a factor of ten reduction in characteristic particle size compared to well annealed single crystal Nb. The thermal hysteresis was also affected by the temperature transition rates, with a significant reduction of the hysteresis for the slowest cooling rates. This implies that at least part of the recorded hysteresis in the well annealed material is dependent on the temperature transition rate.

1. Introduction

The lattice and volume mismatch between a hydride phase and the host lattice affects the precipitation process during cooling and the decomposition process during heating. Stated simply, the formation (or decomposition) of deuteride particles requires additional energy or driving force beyond the free energy of formation (or decomposition). During precipitation, this added driving force is required overcome surface energy associated with the matrix–hydride interface and elastic strain energy associated with the lattice and volume mismatch. The surface energy component can also include dislocation formation energy associated with coherency loss. The observed onset of precipitation, during cooling under constant concentration conditions, will then occur at a temperature below the incoherent solvus temperature. The thermal behaviour associated with hydride decomposition depends on the coherency state of the hydride particles. For completely incoherent particles, the additional energy required for dissolution is expected to be small and dominated by the work of plastic deformation [1]. In this case, the heat-up behaviour will closely approximate the incoherent solvus temperature.

0953-8984/99/387195+16$30.00

The study of hydride formation in Nb is not new and data on the thermal hysteresis in the hydrogen–Nb system exists [2, 3]. One such study is the Rutherford backscattering (RBS) measurements on aligned, single-crystal Nb by Whitton *et al* [2]. The RBS technique has very good sensitivity to hydride formation in single-crystal samples when the incident beam is aligned in a channelling condition. Lattice rotation and dislocation creation associated with hydride precipitation during *in situ* cooling disrupts the channelling process and induces greater RBS yield. The primary result of the work of Whitton *et al* was an accurate measurement of the heat of solution over a concentration range of 2400 to 30 000 atomic parts per million (appm) hydrogen and deuterium. The heat of solution measured by Whitton *et al* during temperature reduction, $\Delta H_c^{solv} = 0.12$ eV, did not exhibit an isotope effect within experimental error [2]. A noticeable thermal hysteresis in the RBS yield was observed, at least for the 9000 appm deuterium measurement shown. This measurement also exhibited the effect of residual dislocations, induced by the first hydride formation cycle, on subsequent hydride nucleation and growth. The effect was to raise the temperature at which hydride precipitation began by 20 degrees [2]. The same effect was also evident in resistivity measurements of Birnbaum *et al* [3]. As with the Whitton *et al* measurement, the onset of precipitation during cooling occurred at a higher temperature than was observed during the first temperature reduction trial.

The utility of small-angle neutron scattering (SANS) in the study of deuteride formation in Nb during cooling was demonstrated in a recent publication [4]. As part of this previous study, the effect of deformation on deuteride formation was investigated in low-concentration Nb–D alloys. Cold rolling was found to significantly affect the deuteride precipitation process, altering the particle morphology and eliminating the thermal hysteresis. These observations were consistent with an elastic interaction between the precipitating deuteride phase and the cellular dislocation substructure facilitating the nucleation process [4]. The measurements presented here extend these initial experiments for a variety of sample treatments.

2. Experimental details

Sample preparation procedures followed those specified in the previous publication [4] and are only briefly outlined here. Single-crystal samples were taken from a 99.9% pure ingot with a [110] cylinder axis supplied by Metal Crystals and Oxides Ltd of Cambridge, England. Polycrystal samples were fabricated from a rod supplied by Johnson Matthey Aesar. The average grain size of this material was determined by etching a polished surface and was found to be approximately 100 μ. Deuterium loading was performed by exposure to D_2 gas at a temperature of 673 K after vacuum annealing at 1073 K. Deuterium concentrations were determined by the volumetric technique and from the change in mass. The concentrations from these two methods typically agreed to within 10%. Deformation was performed by unidirectional rolling at room temperature.

SANS measurements were performed at the Intense Pulsed Neutron Source at Argonne National Laboratory using the small-angle diffractometer (SAD) [5] and the small angle neutron diffractometer (SAND). The performance of each instrument is similar, although the measured Q range of SAND ($0.004 \leqslant Q \leqslant 0.16$ Å^{-1}) is broader than that of SAD ($0.006 \leqslant Q \leqslant$ Å^{-1}). The wavevector transfer, Q, is given by $Q = (4\pi/\lambda)\sin\theta$, where λ is the neutron wavelength and θ is half the scattering angle. Absolute calibration of the macroscopic differential scattering cross section, $\mathrm{d}\Sigma/\mathrm{d}\Omega(Q)$, was determined by using a polymer standard sample [5]. All measurements were performed in vacuum using a Displex as described previously [4]. Sample temperature was recorded with a thermocouple located near the sample on the sample holder.

Table 1. Sample preparation parameters and thermal history.

Sample	Preparation	Thermal history	Solvus temperature[a](K)	Thermal hysteresis data[b]
Nb7 (1)[c]	well annealed 7000 appm	cooling: $\Delta t = 24$ h; $\Delta T/\Delta t = 8\,^{\circ}$C h^{-1} heating: $\Delta t = 6$ h; $\Delta T/\Delta t = 60\,^{\circ}$C h^{-1}	200	$T_c = 170$ K $T_h \sim 240$ K T_R =? (300 K)
Nb7 (2)[c]	cycled once 7000 appm	cooling: $\Delta t = 38$ h; $\Delta T/\Delta t = 4\,^{\circ}$C h^{-1} heating: $\Delta t = 33$ h; $\Delta T/\Delta t = 5\,^{\circ}$C h^{-1}	200	$T_c = 220$ K $T_h = 180$ K $T_R = 280$ K
NbG1	well annealed polycrystal 7600 appm	cooling: $\Delta t = 39$ h; $\Delta T/\Delta t = 5\,^{\circ}$C h^{-1} heating: $\Delta t = 19$ h; $\Delta T/\Delta t = 12\,^{\circ}$C h^{-1}	205	$T_c = 170$ K $T_h = 220$ K $T_R = 280$ K
Nb11(d)[c]	deformed 49.9% (unidirectional) 7700 appm	cooling: $\Delta t = 27$ h; $\Delta T/\Delta t = 8\,^{\circ}$C h^{-1} heating: $\Delta t = 13$ h; $\Delta T/\Delta t = 17\,^{\circ}$C h^{-1}	205	$T_c \sim 240$ K $T_h = 130$ K $T_R \sim 250$ K
Nb12	well annealed 9900 appm	cooling: $\Delta t = 40$ h; $\Delta T/\Delta t = 4\,^{\circ}$C h^{-1} heating: $\Delta t = 19$ h; $\Delta T/\Delta t = 9\,^{\circ}$C h^{-1}	215	$T_c = 180$ K $T_h = 240$ K $T_R = 300$
Nb13	well annealed 8000 appm	cooling: $\Delta t = 58$ h; $\Delta T/\Delta t = 4\,^{\circ}$C h^{-1} heating: $\Delta t = 34$ h; $\Delta T/\Delta t = 7\,^{\circ}$C h^{-1}	205	$T_c = 150$ K $T_h = 150$ K $T_R = 250$ K
Nb14	well annealed 8000 appm	cooling: $\Delta t = 8$ h; $\Delta T/\Delta t = 28\,^{\circ}$C h^{-1} heating: $\Delta t = 32$ h; $\Delta T/\Delta t = 8\,^{\circ}$C h^{-1}	205	directly cooled $T_h = 130$ K $T_R \sim 170$ K

[a] Based on the phase diagram of Smith [6].
[b] T_c, T_h and T_R are the temperatures of deuteride formation, decomposition and complete reversion, respectively (see text).
[c] Numbers in parentheses denote the deuterium loading cycle, while 'd' refers to deformation.

Data are presented for six samples, five single crystal and one polycrystal. One sample was continuously cooled from room temperature to 80 K with a cooling rate of 2–3 K min^{-1}. The other samples were incrementally cooled, with SANS patterns recorded at constant temperature as specified below. All samples were incrementally heated, again with SANS responses recorded at constant temperature. The cooling and heating rates between the constant temperature SANS measurements was approximately 1 K min^{-1}. Sample preparation characteristics, thermal history and the incoherent solvus temperature based on the phase diagram of Smith [6] are listed in table 1. This table also includes data on the overall cooling and heating rates. The overall rates are defined as the total temperature change (ΔT) divided by the total time (Δt) during temperature reduction or elevation, including SANS measurement time. The last column in table 1 lists three temperatures, the temperature at which the onset of precipitation during cooling was observed (T_c), the temperature corresponding to the onset of deuteride decomposition during heating (T_h) and the temperature of complete reversion of the deuteride phase (T_R).

3. Results

3.1. Effect of lattice defects

Materials coherently scatter neutrons in the forward direction (the SANS response) when inhomogeneities are present with sizes of approximately 10 to 2000 Å. Inhomogeneities such as internal voids and second-phase particles (deuterides in particular) are strong scatterers because of the large neutron scattering length contrast relative to the host matrix. Deuterium in solid solution will not result in a coherent neutron scattering response. As demonstrated here and in [4], the SANS signal is a very sensitive monitor of the deuteride precipitation process and can provide particle morphology information. Tracking the SANS response as a function of temperature provides an accurate characterization of the thermal hysteresis.

The treatments of single-crystal material investigated here include deformation by cold rolling and previous deuteride formation. In addition, the effect of grain boundaries on the thermal hysteresis has been investigated. The absolute macroscopic differential scattering cross section, $\mathrm{d}\Sigma/\mathrm{d}\Omega(Q)$, versus Q in ln–ln format for Nb7 near the lower temperature limits of the first (Nb7(1)) and second (Nb7(2)) hysteresis measurement are shown in figure 1. These data are fit with the following cross section,

$$\frac{\mathrm{d}\Sigma}{\mathrm{d}\Omega}(Q) = \frac{4\pi\,\Delta\rho^2}{Q^4}\frac{S}{V} + 2\pi f t\frac{\Delta\rho^2}{Q^2} \tag{1}$$

where the first term is the Porod law and the second term is the single-particle form factor for a plate [7]. In equation (1), S is the total interfacial surface area, V is the irradiated volume, f is the volume fraction of the deuteride phase in the form of small plates, t is the plate thickness

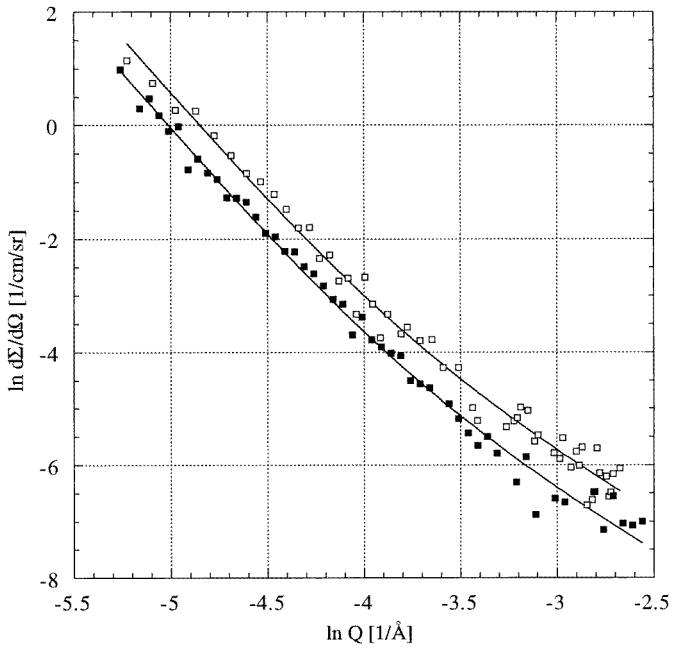

Figure 1. SANS response in ln–ln format near the low-temperature limit of the measured thermal behaviour for Nb7(1) (open boxes) and Nb7(2) (closed boxes). Solid lines are best fits of equation (1) to the data.

Table 2. Parameters describing the deuteride particle morphology derived from low-temperature SANS measurements.

Sample	Q^{-4} amplitude ($\times 10^{-9}$ cm^{-1} Å^{-4} sr^{-1})	S/V (cm^{-1})	$\bar{R}$ (μ)	N_ε (cm^{-3})	Q^{-2} amplitude ($\times 10^{-5}$ cm^{-1} Å^{-2} sr^{-1})	f ($\times 10^{-4}$)
Nb7(1)	2.8 ± 0.4	26.5	11	1.7×10^6	0.7 ± 0.1	6
Nb7(2)	1.8 ± 0.1	17.0	17	0.5×10^6	0.3 ± 0.1	3
Nb12	5.4 ± 0.3	51.1	8	6.4×10^6	0.6 ± 0.1	6
Nb13	4.0 ± 0.5	37.9	8	4.7×10^6	2.8 ± 0.3	25
NbG1	3.3 ± 0.2	31.3	9	3.1×10^6	0.3 ± 0.1	3
Nb11(d)	1.0 ± 0.4	9.5[a]	32[a]	7×10^{4}[a]	3.6 ± 0.2	32
Nb14	25.4 ± 0.9	241	1(.3)	1.1×10^9	—[b]	—
Nb1[c]	22.6 ± 1.0	214	1(.4)	0.9×10^9	—[b]	—

[a] Deformation significantly alters particle morphology [4]. An additional uncertainty is therefore associated with derivation of these parameters through the application of equations (1) and (4). See text for discussion.
[b] The directly cooled samples do not exhibit the Q^{-2} behaviour at highest Q.
[c] Data reproduced from [4] and included here for comparison.

and $\Delta\rho$ is the scattering length contrast, in the present case between the ε deuteride phase and the Nb solid solution α phase ($\Delta\rho \cong 2.9 \times 10^{10}$ cm^{-2}). Although some uncertainty in the Nb–H phase map exists [6], the low-temperature, low-concentration phase is referred to as 'ε' here. The ε phase is an ordered phase with an Nb_4D_3 composition and an orthorhombic unit cell [6]. A 12% volume expansion accompanies the $\alpha \rightarrow \varepsilon$ incoherent phase transformation.

As with previous measurements in [4], the scattering response from all undeformed samples was isotropic. The Porod response is an asymptotic behaviour valid for all Q such that $Q\mathcal{D} \gg 1$, where $\mathcal{D}$ is the characteristic dimension of the scattering object [7, 8]. Based on the isotropic nature of the response and previous TEM investigations [3, 9, 10], the Porod response is attributed to large spherical deuteride particles ($\mathcal{D} \sim 2000$ Å or greater) [4]. On the other hand, the plate form factor observed at higher Q is the result of a much smaller set of deuteride particles ($t \sim 20$ Å) with a platelike morphology (referred to as the 'small-plate' particles below). The Q^{-4} and Q^{-2} amplitudes, S/V ratios and f obtained from the fit of equation (1) to the data in figure 1 are listed in table 2 along with the measurements of other samples, as discussed below. A small-plate thickness of 20 Å was assumed in the calculation of f. As discussed in detail in [4], the small-plate scattering response must satisfy $Qt \leqslant 1$ at the high-Q limit of the SANS measurement, leading to an estimated maximum thickness of approximately 20 Å.

The normalized variation of the Porod amplitude with temperature for the first and second thermal cycles of Nb7 is shown in figure 2. (The Q^{-2} components of the undeformed samples reported on here were too weak to accurately characterize as a function of temperature.) The effect of the first cycle on the thermal hysteresis of the second cycle is clear. The significant reduction of the hysteresis is attributed to the preferential nucleation of the deuteride phase on residual dislocations left behind by the first thermal cycle. Preferential low-temperature hydride (deuteride) formation at residual dislocations, previously observed with TEM by Schober [9], is consistent with local lattice disorder reducing the free energy nucleation barrier.

Grain boundaries, on the other hand, do not alter the thermal hysteresis. The temperature dependence of the normalized Porod amplitudes for the first thermal cycles of NbG1 (undeformed, polycrystal with 7000 appm deuterium) and Nb7 are shown in figure 3. The similarity of the two thermal behaviours is a strong indication that preferred nucleation of the deuteride phase at grain boundaries does not occur, at least within the ability of the SANS measurement to characterize this component of the precipitating phase. The consistency of

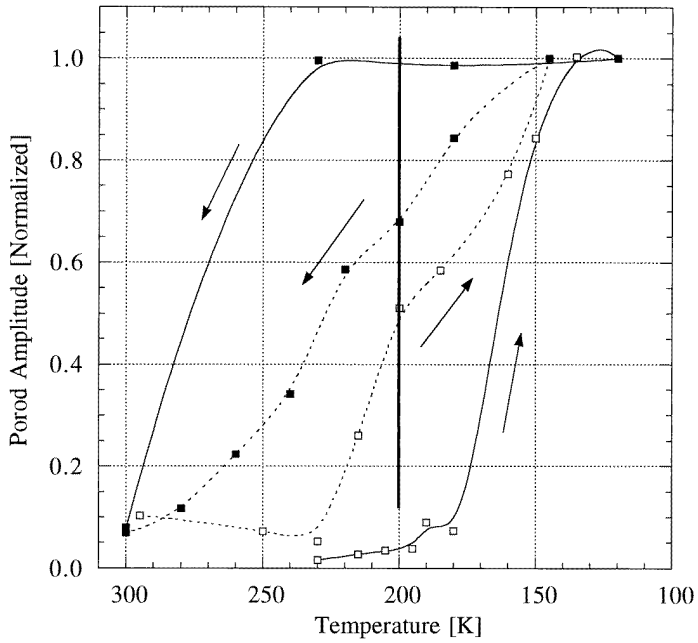

Figure 2. Normalized Porod amplitude versus sample temperature during cooling (open boxes) and heating (closed boxes) for the first (solid lines) and second (dotted lines) cycles of Nb7. The equilibrium, incoherent solvus temperature is represented by the vertical line.

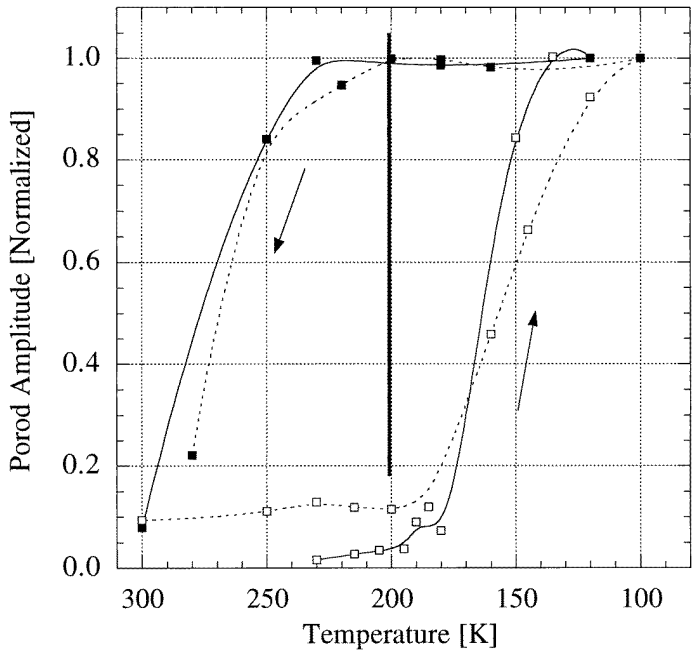

Figure 3. Normalized Porod amplitude versus sample temperature during cooling (open boxes) and heating (closed boxes) for the Nb7(1) (solid lines) and NbG1 (dotted lines). The equilibrium, incoherent solvus temperature is represented by the vertical line.

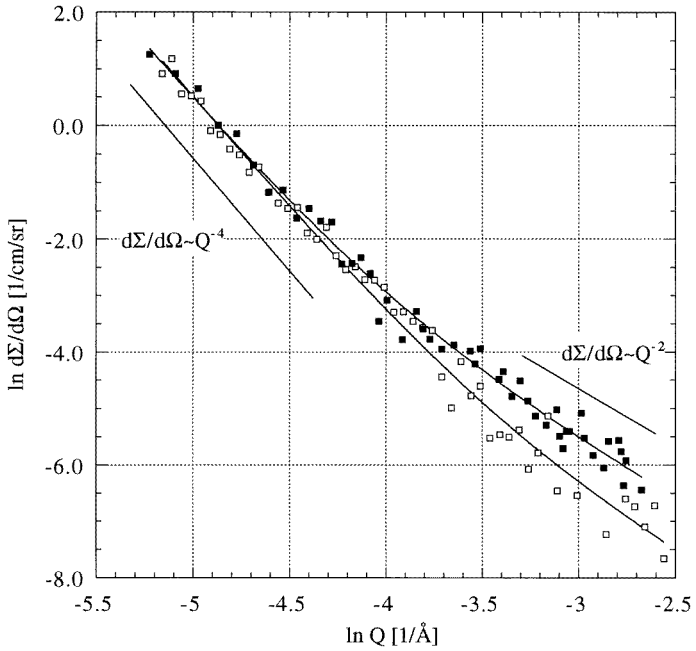

Figure 4. SANS response in ln–ln format near the low-temperature limit of the measured thermal behaviour for NbG1 (open boxes) and Nb7(1) (closed boxes). Solid lines are best fits of equation (1) to the data.

these behaviours is reaffirmed by the scattering cross section measurements of each at the lower temperature limit of the thermal hysteresis, shown in figure 4. The parameters from the fit of equation (1) to the NbG1 SANS measurement are included in table 2. Notice that Q^{-4} amplitudes for NbG1 and Nb7(1) are equal within statistical uncertainty.

Grain boundaries can act as preferred sites, promoting heterogeneous nucleation [11]. The indifference of thermal behaviours in figure 3 to this effect could therefore be considered unexpected. However, the fraction of Nb atoms associated with the grain boundary area is minute; only 3×10^{-4} of the atoms are within 50 Å of the grain boundary interfaces in a 100 μ grain size sample. One might expect a similar fraction of the deuteride particles to nucleate at grain boundaries and this could very well be beyond the sensitivity of a SANS measurement. The argument can be made, however, that the *growth* of inter-granular deuteride particles would be favoured over the *nucleation* of intra-granular particles, at least insofar as diffusion-based transport would allow. If this argument does hold, then the observed thermal hysteresis should be reduced by the presence of grain boundaries.

The effect of deformation by cold rolling is shown in figure 5, the first-cycle thermal behaviour of Nb11(d) (deformed, 7700 appm deuterium), again compared with Nb7(1). As expect, the thermal hysteresis is completely eliminated by deformation. A further point of comparison is shown in figure 6, the SANS responses from Nb11(d) and Nb7(1) at the lower temperature limit. The low-temperature scattering response of Nb11(d) is noticeably larger at high Q. This is apparent in the Q^{-2} amplitude for Nb11(d) listed in table 2. The magnitude of the Q^{-2} response from the deformed sample is sufficiently large, consistent with earlier measurements [4], to permit an analysis of the thermal behaviour of the small-plate deuteride particles. This is shown in figure 7, where the thermal behaviours of the Q^{-2} and Q^{-4}

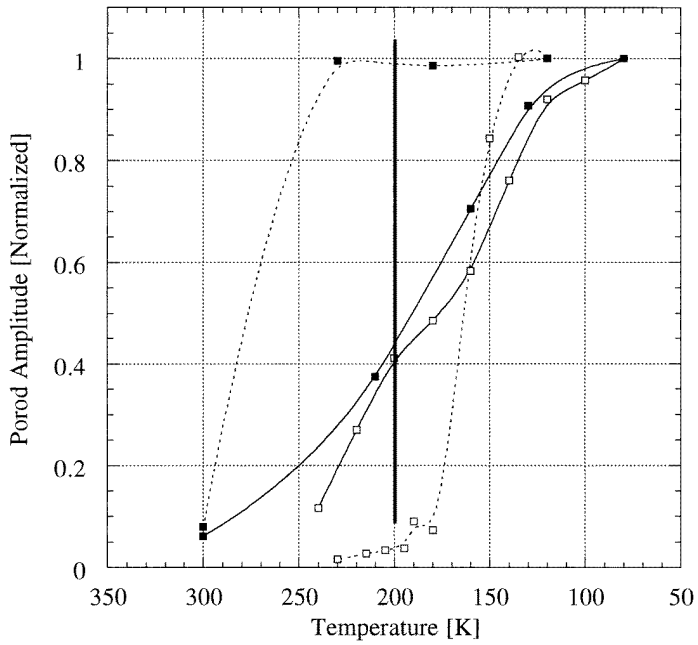

Figure 5. Normalized Porod amplitude versus sample temperature during cooling (open boxes) and heating (closed boxes) for Nb11(d) (solid lines) and Nb7(1) (dotted lines). The equilibrium, incoherent solvus temperature is represented by the vertical line.

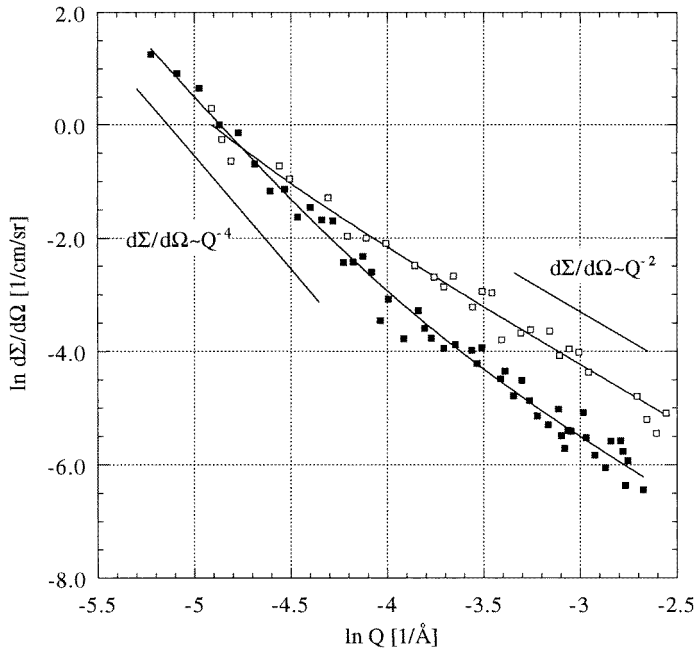

Figure 6. SANS response in ln–ln format near the low-temperature limit of the measured thermal behaviour for Nb11(d) (open boxes) and Nb7(1) (closed boxes). Solid lines are best fits of equation (1) to the data.

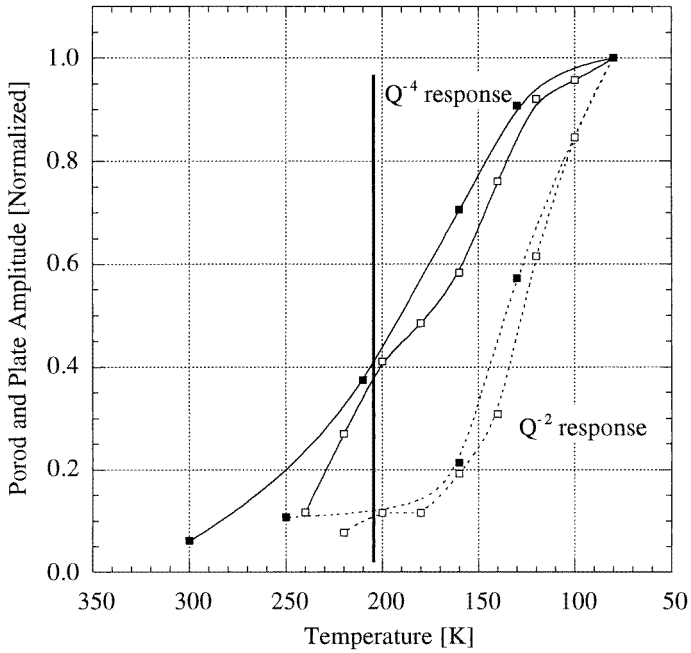

Figure 7. Normalized Porod amplitude versus sample temperature during cooling (open boxes) and heating (closed boxes) for the Porod (solid lines) and small-plate (dotted lines) responses from Nb11(d). The equilibrium, incoherent solvus temperature is represented by the vertical line.

responses are plotted together. Like the Q^{-4} behaviour, the Q^{-2} response does not exhibit a hysteresis. In addition, the precipitation of the small plate component responds to a solvus temperature reduced by approximately 50 degrees. Similar observations were made with a high-concentration, deformed sample loaded to 24 500 appm [4]. We suspect this is the result of low deuterium concentration in solid solution (hence the lower solvus temperature) after the precipitation of the larger deuteride particles. We do not have an explanation of why the precipitation of small-plate component occurs after that of the much larger Porod particles.

3.2. Effect of temperature transition rates

The effect of sample cooling rate on the deuteride decomposition was investigated by using two different *in situ* cooling rates, continuously cooled and step-wise cooled. The purpose of these experiments was to investigate the effect of deuteride precipitate size on the decomposition process, as characterized by the thermal behaviour of the scattering response during heating. As has been previously observed, continuous cooling results in a smaller mean deuteride particle size [4], an affect attributed to more rapid undercooling favouring nucleation over growth. Conversely, a slow transition across the solvus temperature allows more time for nucleation (which is inhibited because of the smaller undercooling) and growth (promoted by greater diffusion at higher temperatures). This is expected to result in a coarser deuteride particle distribution.

The normalized Porod responses of two undeformed, single-crystal samples, Nb13 (8000 appm deuterium), and Nb14 (8000 appm deuterium), are shown in figure 8. The cooling branch for Nb14 was not recorded because of continuous cooling to 80 K. The SANS cross sections of Nb13 and Nb14 at 80 K are shown in figure 9. The response of Nb13 (step-wise

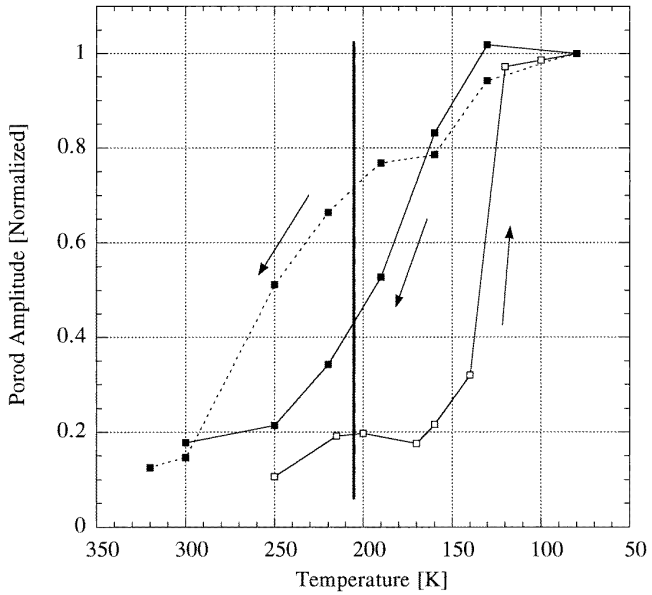

Figure 8. Normalized Porod amplitude versus sample temperature during cooling (open boxes) and heating (closed boxes) for the Nb13 (solid lines) and Nb14 (dotted line). The equilibrium, incoherent solvus temperature is represented by the vertical line. The Nb14 cooling branch was not recorded because of direct cooling to 80 K.

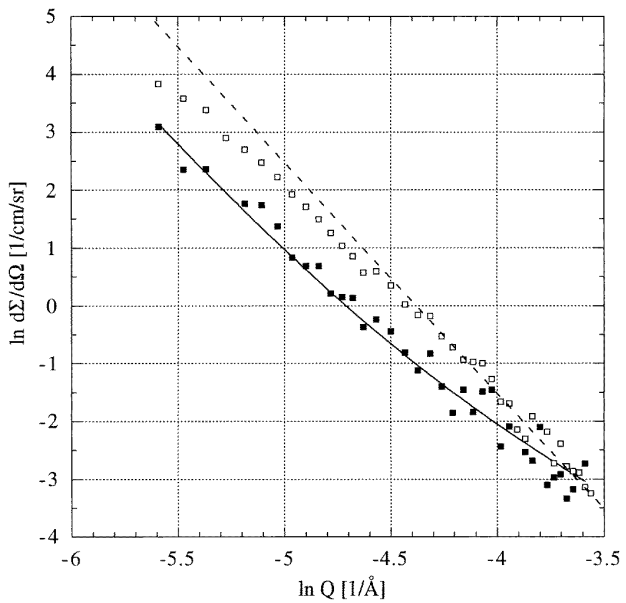

Figure 9. SANS response in ln–ln format near the low-temperature limit of the measured thermal behaviour for Nb14 (open boxes) and Nb13 (closed boxes). The solid line is a best fit of equation (1) to the Nb13 data. The dotted line is the Porod law fitted to the Nb14 high-Q data and extrapolated to low Q. The divergence of the data and extrapolation is a particle size effect; the direct quenching procedure induced a finer deuteride dispersion, resulting in the observed fall-off from the Porod law at lower Q.

cooling) is fitted with equation (1) over the entire measured Q range. The response of Nb14, on the other hand, falls off from the Porod law below $Q \sim 0.014$ Å^{-1}. This roll-over effect is the result of a smaller mean particle, and as explained above, is due to the direct cooling procedure.

The hysteresis of Nb13 is reduced compared to that of the other undeformed samples, an effect attributed to slower cooling and heating rates (see table 1). This is shown explicitly in figure 10, the thermal behaviour for Nb7(1) (most rapid rates), Nb12 (intermediate rates), and Nb13 (slowest rates). The thermal behaviour for Nb13 has been shifted by 50 degrees in figure 10 for comparison purposes. (The $\mathrm{d}\Sigma/\mathrm{d}\Omega$ versus Q data of Nb12 are similar to the other undeformed samples and not shown. The scattering amplitudes at the low-temperature limit are listed in table 2.) The reduction of the thermal hysteresis as the temperature transition rates are reduced implies that at least part of the observed hysteretic behaviour is the result of insufficient time during cooling and heating. This point has been made by Westlake and Ockers [12].

4. Analysis and discussion

4.1. Deuteride precipitate size

The two SANS behaviours given in equation (1) are both sensitive to the precipitate size. First, the exact plate form factor (the Q^{-2} power law) includes an exponential modifier, $\exp(-Q^2t/12)$, that accounts for a non-zero plate thickness. We omitted this term in data fitting because the correction is obscured by the incoherent background and poor counting statistics at high Q. Furthermore, the volume fraction of the small-plate component of the deuteride phase, f, determined by the fit of equation (1) and shown in table 2, is very small. (For comparison, the total volume fraction of the ε phase determined by the lever rule is approximately 0.02 for all samples presented here.) Thus, the majority of the deuteride phase consists of the large spherical particles causing the low-Q Porod scattering. It was for this reason that the Porod response is used as a monitor of the thermal precipitation behaviour.

The Porod scattering behaviour, via the S/V ratio, is also correlated to the precipitate size. If the overall deuterium concentration is known, a pair of equations can be solved to yield a characteristic radius. First, S/V is given by

$$\frac{S}{V} = \int 4\pi R^2 N(R)\,\mathrm{d}R \approx 4\pi \bar{R}^2 N_\varepsilon \tag{2}$$

where $\bar{R}$ is the characteristic radius, $N(R)$ is the differential deuteride particle size distribution and N_ε is the effective number of deuteride particles per unit volume assuming all are of size $\bar{R}$. The right-hand side of equation (2) is an obvious assumption. It is justified here since we have no *a priori* knowledge of the true distribution and since our purpose is only to extract a characteristic precipitate size that meets the surface area and concentration constraints. A second equation can be written for the total deuterium loading,

$$N_D = \frac{3}{4} N_{Nb} \int \frac{4}{3}\pi R^3 N(R)\,\mathrm{d}R \approx \pi N_{Nb} \bar{R}^3 N_\varepsilon \tag{3}$$

where N_D and N_{Nb} are, respectively, the deuterium and niobium number densities of the ε phase. We again assume a monodispersed deuteride particle distribution. We also assume that all deuterium is in the ε phase (for all practical purposes, deuterium is completely immiscible in Nb below 150 K [6]) and that this phase consists entirely of large spherical particles (at most a 10% error, see values of f in table 2). Equations (2) and (3) can be solved for $\bar{R}$,

$$\bar{R} = \frac{4N_D}{N_{Nb}} \left(\frac{S}{V}\right)^{-1}. \tag{4}$$

The characteristic radii obtained from equation (4) and effective particle number densities, N_ε, obtained from equation (2) (or equivalently, equation (3)) are listed in table 2. We emphasize that these parameters are obtained under the approximations discussed above for the purpose of qualifying the effect of sample preparation and thermal history on precipitate size and number density.

A few interesting trends are evident in table 2. First, the deuteride particle radii and number densities for the first cycles of all step-wise cooled samples except Nb11(d) are about equal. This is to be expected since the samples were loaded to approximately the same deuterium concentration and were cooled with roughly equivalent rates. Previous deuteride cycling results in a significant increase of the characteristic size, as seen by a comparison of the first and second cycles of Nb7. This is consistent with the observed thermal behaviour of the second cycle; precipitation occurred at a temperature much closer to the solvus line, allowing for greater growth and a corresponding smaller number of particles. The effect of direct versus step-wise cooling can be seen by comparing Nb13 (step-wise) with Nb14 (direct). As discussed above, the direct cooling procedure was expected to result in a much finer dispersion (greater number of smaller particles). This is indeed the case. In addition, a second well annealed, single crystal sample, Nb1, was directly cooled from room temperature to 120 K for a single SANS measurement as part of previous study [4]. This sample was loaded with 7400 appm deuterium. The corresponding characteristic radius and number density are nearly equal to that of Nb14. Based on the consistency of the Nb14 and Nb1 radii, we believe that the 1 μ plus particle size is the minimum obtainable by direct cooling at the 2–3 $^\circ$C min^{-1} rate used here.

The Nb11(d) radius and number density deserve further discussion. Deformation significantly alters the deuteride particle morphology, causing the formation of large, highly anisometric plates [4]. While asymptotic Porod scattering still occurs, equation (1) is no longer valid in the strictest sense [8]. An additional uncertainty is then associated with the application of equation (4) to these data. The characteristic deuteride radius and number density that follow must be considered with this in mind. That stated, we note the trend represented by the Nb11(d) is consistent with the elimination of the thermal hysteresis; as with cycling, deformation facilitates precipitation and results in a smaller number of larger particles.

4.2. Thermal hysteresis

An expression for the thermal hysteresis, $\Delta T/T$, can be derived as follows. The measured hydrogen (or deuterium) terminal solid solubility upon cooling, C_c, and heating, C_h, are given by

$$\begin{aligned} C_c &= \exp(\Delta S_{\alpha\to\varepsilon}/k)\exp(-\Delta H_c^{solv}/kT_c) \\ C_h &= \exp(-\Delta S_{\varepsilon\to\alpha}/k)\exp(\Delta H_h^{solv}/kT_h) \end{aligned} \tag{5}$$

where $\Delta S_{\alpha\to\varepsilon}$ and $\Delta S_{\varepsilon\to\alpha}$ are the entropies of ε phase formation and decomposition, respectively, ΔH_h^{solv} and ΔH_c^{solv} are the heats of solution during cooling and heating, respectively, and T_c and T_h are the measured solvus temperatures during cooling and heating, respectively. The thermal hysteresis, measured under constant concentration conditions, is then given by

$$\begin{aligned} \frac{\Delta T}{T} = \frac{T_h - T_c}{T_c} &= \frac{1}{\Delta H_c^{solv}} kT_h \left(\frac{\Delta S_{\alpha\to\varepsilon}}{k} + \frac{\Delta S_{\varepsilon\to\alpha}}{k} \right) - \Delta H_h^{solv} - \Delta H_c^{solv} \\ &\simeq \frac{-\Delta H_h^{solv} - \Delta H_c^{solv}}{\Delta H_c^{solv}}. \end{aligned} \tag{6}$$

The RHS of this equation is written under the assumption that $\Delta S_{\alpha\to\varepsilon} = -\Delta S_{\varepsilon\to\alpha}$. The relationship between the heats of solution and the thermal hysteresis is given by

$$-(\Delta H_h^{solv} + \Delta H_c^{solv}) \cong \Delta H_c^{solv}\frac{\Delta T}{T} = 0.12\ (\mathrm{eV})\frac{\Delta T}{T} \tag{7}$$

where we assume the Whitton *et al* heat of solution measurement in single crystal Nb is representative of our work as well. The measured thermal hysteresis and difference in the heats of solution given by equation (7) for the first cycle of all undeformed, step-wise cooled samples are listed in table 3. The thermal hysteresis given by the LHS of equation (6) is undefined, or the data does not exist, for the remaining samples (see below).

Table 3. Thermal hysteresis and heat of solution parameters.

Sample	$\Delta T/T$ [a]	$-(\Delta H_h^{solv} + \Delta H_c^{solv})$ (eV)
Nb7(1)	0.4 ± 0.2	0.05 ± 0.02
NbG1	0.3 ± 0.1	0.04 ± 0.01
Nb12	0.3 ± 0.1	0.04 ± 0.01
Nb13	0 ± 0.1	0 ± 0.01

[a] Errors are based on uncertainties of T_c and T_h estimated from the Porod thermal behaviour.

The difference in heats of solution has been attributed to the work of plastic deformation associated with hydride formation and decomposition [3, 13]. This model was later revised by Puls [1] with consideration of the plastic–elastic calculations of Lee *et al* [14] and Earmme *et al* [15]. We summarize this work here. For an ideally plastic material such as a well annealed metal, very little elastic accommodation energy is available—because the host plastically deforms, relieving much of the elastic energy—to aid the decomposition of micron-sized or larger hydride precipitates. The heat-up branch should then approximate the equilibrium, incoherent solvus, while the cool-down branch is dominated by the elastic accommodation and surface energy associated with hydride nucleation. A highly work-hardened material, on the other hand, will not be able to undergo plastic deformation to relieve the elastic accommodation energy. In this case, the elastic energy is available for hydride dissolution and the thermal hysteresis is expected to be small.

We present thermal hysteresis data for two classes of samples, undeformed (those listed in table 3) and deformed (Nb7(2) and Nb11(d)). (Hysteresis data for Nb14 do not exist because of the direct cooling procedure.) First, the heat-up branches of the deformed set, especially Nb11(d), track closely with the cool-down branches, effectively invalidating the above thermal hysteresis analysis since $\Delta T/T < 0$. This observation is consistent with reversible elastic accommodation energy available at the very beginning stages of dissolution, resulting in deuteride decomposition at the onset of the heat-up measurement. As discussed in the previous paragraph, this is the expected behaviour of dissolution in a heavily strain hardened matrix.

The remaining undeformed samples listed in table 3 present a interesting contrast. Recall Nb13 underwent a prolonged cooling procedure to induce greater deuteride growth during cooling. The Porod amplitude of this sample decreased as the solvus temperature is crossed upon heating (the only undeformed sample observed to behave this way). This is a strong indication that at least some of the hydride particles were large and incoherent. In this case, the heat-up branch is expected to response to the incoherent solvus temperature, without significant superheating, as observed. (That differences in the particle growth are not borne out in the characteristic radii is evidence of the underlying assumptions used in the derivation of equation (4).) The elimination of the thermal hysteresis for Nb13, at least insofar as

$\Delta T/T \sim 0$, is also consistent with a more equilibrium behaviour during cooling and heating. The thermal hystereses of the remaining undeformed samples are finite and equal within statistical uncertainty. The difference in heats of solution for Nb7(1), NbG1 and Nb12 determined from equation (7) are also consistent with the resistivity measurement of a 1 at.% Nb–H alloy by Birnbaum *et al*, $-(\Delta H_h^{solv} + \Delta H_c^{solv}) \cong 0.02$ eV [3]. Given the behaviour of Nb13, we suspect that the thermal behaviours of Nb7(1), NbG1 and Nb12 were influenced by the temperature transition rates, especially during heating.

5. Conclusions

Deuteride formation in low-concentration (less than 1 at.%) single and polycrystal Nb alloys has been monitored with *in situ* SANS. The effect of deformation, grain boundaries, and temperature transition rates on deuteride particle morphology and on the thermal hysteresis have been investigated. The following conclusions are based on the analysis of the SANS data:

(i) Dislocations produced by cold rolling and by deuteride cycling in single crystal Nb had a pronounced effect on the thermal hysteresis behaviour and the deuteride particle morphology. Cold rolling completely eliminated the thermal hysteresis and induced measurable precipitation as the solvus temperature was crossed during cooling. This is in contrast to the well annealed single crystal samples which are characterized by a large hysteresis and required significant undercooling to induced precipitation. This contrasting behaviour is attributed to dislocation defects facilitating a more heterogeneous precipitation process in the cold rolled sample. A coarser deuteride particle distribution (smaller number of larger precipitates) was observed for the cold rolled sample. This is also consistent with heterogeneous nucleation enabling greater particle growth.

The heating branch of the cold rolled sample tracked closely to the cooling branch. This behaviour was not observed in the well annealed samples. The initiation of the dissolution process upon first heating is the expected response of a heavily work hardened matrix; the deuteride particles retain elastic accommodation energy, because the work hardened host matrix cannot plastically deform, and this energy is available for dissolution at the onset of heating.

Deuteride precipitation in the previously cycled sample is similar to that in the cold rolled sample; a coarser particle distribution and significant reduction in the thermal hysteresis were observed. However, the extent of these trends was not as great as with the cold rolled sample. This may be an indication that the dislocation substructure in the cycled sample is not as efficient at facilitating heterogeneous precipitation and resisting plastic deformation. The dislocation substructures that evolve during cold rolling and deuteride cycling are very different. A heterogeneous, cellular pattern often develops in heavily worked metals, while hydride cycling creates a more uniform substructure as the phase boundary progresses through the matrix. The interactions between the precipitating deuteride phase and the long-range elastic stress fields associated with a cellular dislocation structure may very well be stronger, leading to the observed behaviour.

(ii) The particle morphology and thermal hysteresis of the well annealed polycrystal sample were similar to those of the well annealed single crystal samples. Although the lattice disorder associated with grain boundaries might be expected to influence the precipitation process, this evidently does not occur. The absence of local or heterogeneous nucleation at grain boundaries has been noted by Birnbaum *et al* in a TEM study of hydride precipitation in low-concentration Nb–H alloys [3]. Our result is consistent with this previous observation.

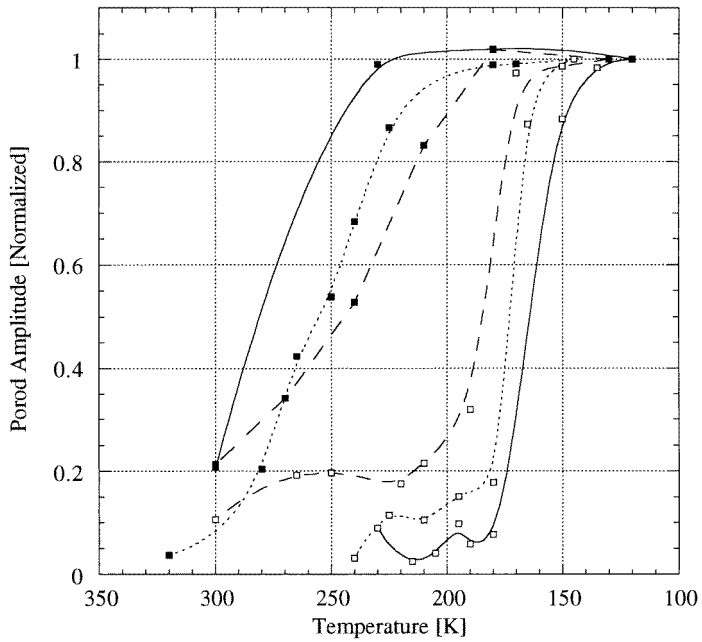

Figure 10. Normalized Porod amplitude versus sample temperature during cooling (open boxes) and heating (closed boxes) for Nb7(1) (solid lines), Nb12 (dotted lines) and Nb13 (dashed lines). The Nb13 data have been shifted by 50 degrees for comparison purposes. The reduction of the hysteresis from Nb7(1) to Nb13 is due, in part, to the temperature transition rates used (see text).

(iii) Temperature transition rates had a noticeable effect on the deuteride particle morphology and thermal hysteresis in well annealed, single crystal Nb. Rapid, direct cooling induced a much finer deuteride particle distribution, resulting in a factor of 200 increase in the effective number density and a factor of 10 reduction in the characteristic particle size compared to the step-wise cooled samples. The dissolution process in the sample with the slowest temperature transition rates was observed to begin at the solvus temperature upon heating, a behaviour unique among the well annealed samples. This is attributed to the dissolution of large deuteride particles that experienced nearly complete elastic stress relief upon growth. The thermal hysteresis, defined as $\Delta T/T$ by equation (6), was eliminated by the very slow, step-wise cooling procedure. Based on this result, we believe the finite thermal hystereses observed for the other well annealed samples are due, in part, to the temperature transition rates.

Acknowledgments

The authors acknowledge the support of the National Science Foundation under grant No DMR-9496297. The SANS measurements were performed at the Intense Pulsed Neutron Source at Argonne National Laboratory. This facility is supported by the US DOE, BES-Materials Sciences, under contract No W-31-109-ENG-38. We also appreciate the assistance given to us by Mr D Wozniak (IPNS-ANL).

References

[1] Puls M P 1984 *Acta Metall.* **32** 1259–69
[2] Whitton J L, Mitchell J B, Schober T and Wenzl H 1976 *Acta Metall.* **24** 483–90
[3] Birnbaum H K, Grossbeck M L and Amano M 1976 *J. Less-Common Met.* **49** 357–70
[4] Heuser B J and Althauser J W 1997 *J. Phys.: Condens. Matter* **9** 8945–61
[5] Thiyagarajan P, Epperson J E, Crawford R K, Carpenter J M, Klippert T E and Wozniak D G 1997 *J. Appl. Crystallogr.* **30** 280–93
[6] Smith J F 1983 *Bull. Alloy Phase Diagr.* **4** 39–46
[7] Porod G 1982 *Small Angle X-Ray Scattering* ed O Glatter and O Kratky (London: Academic) p 17–51
[8] Roth M 1977 *J. Appl. Cryst.* **10** 172–6
[9] Schober T 1975 *Phys. Status Solidi* a **30** 107–16
[10] Schober T 1975 *Phys. Status Solidi* a **29** 395–406
[11] Porter D A and Easterling K E 1992 *Phase Transformations in Metals and Alloys* (London: Chapman and Hall)
[12] Westlake D G and Ockers S T 1975 *Metall. Trans.* A **6** 399–402
[13] Puls M P 1981 *Acta Metall.* **29** 1961–8
[14] Lee J K, Earmme Y Y, Aaronson H I and Russel K C 1980 *Metall. Trans.* A **11** 1837–47
[15] Earmme Y Y, Johnson W C and Lee J K 1981 *Metall. Trans.* A **12** 1521–30